

# Structure of Hybrid Colloid–Polymer Xerogels

Luis Esquivias,<sup>\*,†</sup> Nicolás de la Rosa-Fox,<sup>†</sup> Mercedes Bejarano,<sup>‡</sup> and María J. Mosquera<sup>‡</sup>

*Departamento de Física de la Materia Condensada, Departamento de Química-Física, Facultad de Ciencias, Universidad de Cádiz, 11510 Puerto Real, Spain*

*Received July 10, 2003. In Final Form: January 22, 2004*

Crack-free monolithic gels were prepared from different mixtures of colloidal silica with a sol solution containing tetraethoxysilane, under powerful ultrasonic agitation (sonosol). Recently, information on the structure of these gels, inferred from N<sub>2</sub> adsorption and mercury intrusion porosimetry, was presented. In the present paper, these data were used to construct structural models of the gels using Monte Carlo calculations on the basis of random close packing (RPC) premises. In addition, the structure of gels under study was investigated by transmission and scanning electron microscopy. The material can be described as a composite in which the sonogel is the matrix and the colloid particles the reinforcing phase. For low colloid content, the colloid forms discrete clusters, and the main structural characteristic of sonogels, i.e., a network of uniformly sized particles of ~3–4-nm radius, remains unmodified. However, for high colloid silica content, a multimode distribution appears, the structure is discontinuous, and only colloid aggregates larger than 100 nm are observed. For medium colloid content, aggregates of ~50–100 nm can be seen, but the sonogel structure extends throughout the whole material. By the processing method and election of a suitable precursor concentration, it is possible to design the composite for specific purposes.

## Introduction

Gels are often classified either as *polymeric* or *particulate*.<sup>1,2</sup> Use of the term polymeric is usually limited to those gels obtained by hydrolysis of metallorganic compounds in alcohol solution and polymerization of the resulting products, whereas the term particulate is used to identify those gels obtained by destabilization of an aqueous colloidal solution of oxides, hydroxides, or mineral salts. The method, precursors, and catalyst used have a profound effect on their *structure*, using the term structure to refer to the mutual disposition of solid and fluid phases. Destabilization of colloids gives rise to a uniform structure built by the agglomeration of the colloid particles. The size and distribution of these agglomerates depends on the temperature and pH of the solution.

One way of preparing a polymeric gel is exposing a mixture of alkoxide and water to intense ultrasound.<sup>3–5</sup> This method does not require adding a common solvent (generally methyl or ethyl alcohol) to ensure homogeneous mixing of the alkoxide–water system. These gels are usually called *sonogels*; they are dense and their structure is fine and homogeneous, not only because there is no solvent needed to obtain the sol but also, and mainly, because of the initial cross-linked state of reticulation induced by ultrasound. Another special characteristic of these gels after drying is that the resulting sonogels

present a particulate structure,<sup>6</sup> unlike their counterparts obtained without applying ultrasound, which are filamentous. This particular structural characteristic facilitates the study of their structure, provided an adequate strategy is adopted.

It is commonly asserted that an attractive feature of sol–gel processing is the possibility of tailoring unique materials. The combination of two particulate materials with processing methods that allow full intermingling of both structures has driven our interest in colloid–polymer hybrid gels. This paper describes the preparation of SiO<sub>2</sub>/SiO<sub>2</sub> composites for the purpose of producing bulk materials from gels while avoiding the cracking that can occur during drying. The intention is to tailor a structure in which the small particles generated by the sonogel process modify the uniform structure, which is characteristic of the colloid gels. In a previous paper we have presented a preliminary structural study<sup>7</sup> in which we verified that addition of colloid silica particles to TEOS-based alkogels enables the network porous volume and pore radius to be tailored. Further, we verified that the increase in network pore size, produced by the colloid addition, permitted a significant reduction of the capillary pressure during drying, favoring monolith production. Another consequence was that, using this method, materials could be produced that present a mechanical behavior different from that of other gels. Usually, mesoporous gels, such as light aerogels, are highly compliant materials, with a pore structure that collapses when they are severely compressed under Hg isostatic pressure. Thus mercury does not intrude into their pore structure. In the case of the hybrids under study, although they are mesoporous, they are also stiff enough to allow intrusion. This combination of large pore size/low compliance is infrequently required.

\* Corresponding author: E-mail address: luis.esquivias@uca.es. Telephone: +34-956016321. Fax: +34-956016288.

<sup>†</sup> Departamento de Física de la Materia Condensada.

<sup>‡</sup> Departamento de Química-Física.

(1) Flory, P. J. *Faraday Discuss. Chem. Soc.* **1974**, *57*, 7.

(2) Rabinovich, E. M. In *Sol–gel Technology for Thin Films, Fibers, Preforms, Electronics and Special Shapes*; Klein, L. C., ed.; Noyes: Park Ridge, NJ, 1988; p 260.

(3) Zarzycki, J. *Heterogeneous Chem. Rev.* **1994**, *1*, 243.

(4) Blanco, E.; Esquivias, L.; Litrán, R.; Piñero, M.; Ramírez-del-Solar, M.; de la Rosa-Fox, N. *Appl. Organomet. Chem.* **1999**, *13*, 399.

(5) de la Rosa-Fox, N.; Esquivias, L.; Piñero, M. *Organic–Inorganic Hybrid Materials from Sonogels*. In *Handbook of Organic–Inorganic Hybrid Materials and Nanocomposites*; Nalwa, S. H., Ed.; American Scientific Publishers: CA, 2003; Vol. 1, pp 241–270.

(6) Esquivias, L.; González-Peccei, A.; Rodríguez-Ortega, J.; Barrera-Solano, C.; de la Rosa-Fox, N. *Ceram. Trans.* **1998**, *95*, 183.

(7) Mosquera, M. J.; Bejarano, M.; De la Rosa-Fox, N.; Esquivias, L. *Langmuir* **2003**, *19*, 951.

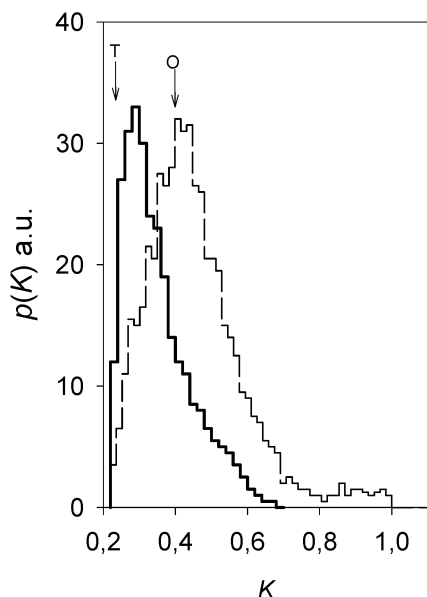


**Figure 1.** Interstice distribution  $p(K)$  in a RCP of identical spheres: Frost distribution (continuous line); Scott loose distribution (dashed line). The variable  $K = r/R$ , where  $r$  is the radius of the largest inscribed sphere in the interstice and  $R$  the radius of the particles (T, tetrahedral sites; O, octahedral sites).<sup>12,13</sup>

The goal of this paper is to describe the gel structure, as a prior step to establishing a relationship between texture and mechanical behavior. The xerogel structure has been depicted as a hierarchy of several levels by means of models built up using the Monte Carlo calculations, on the basis of random close packing (RCP) premises.<sup>8–11</sup> Here we expect to find two structures sharing the same space but that can be studied separately, under these hypotheses.

**Description of the Structural Approach.** Electronic microscope observations of sonogels suggest that the sonogel structure is a dense assemblage of almost monosized particles and only locally contains larger pores. Alternatively, adsorption studies show a quite narrow pore size distribution followed by a slim tail of larger (macro) pores. The main contribution to specific surface arises from mesoporosity. The approach conceived for this structural study was, ideally, to discount the macropores and describe the remaining structure in terms of an RCP model. To test the degree of applicability of such a model, Zarzycki<sup>8,9</sup> found a link between the “particle space” and “pore space” data. Frost<sup>12</sup> and Finney and Wallace<sup>13,14</sup> provided the distribution of the largest sphere radii inscribed in the interstices of several RCP models previously studied by Bernal and Mason<sup>15</sup> and Scott.<sup>16</sup> Figure 1 shows these distributions,  $p(K)$ , plotted as the function of a reduced variable  $K = r/R$ , where  $r$  is the radius of the largest inscribed sphere and  $R$  the particle radius, in the hypothesis of hard-sphere approximation. The largest

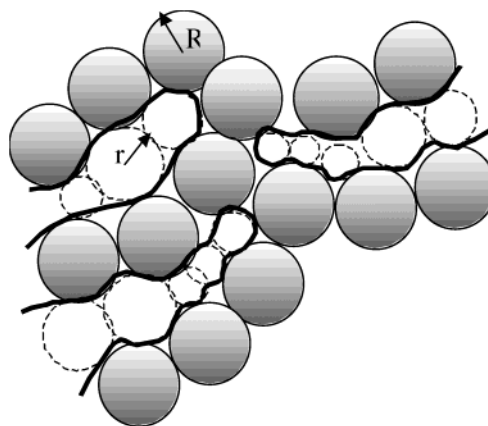


**Figure 2.** Estimation of the pore dimension by a sequence of inscribed spheres of variable radius,  $r$ , in an assembly of spheres of fixed radius,  $R$ .

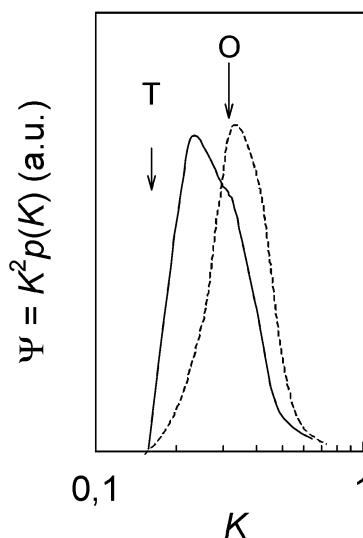


**Figure 3.** Volume derivative distributions  $\Psi(K) = K^2 p(K)$  as a function of  $\log K$  corresponding to the Frost (continuous line) and Scott (dashed line) loose distributions (T, tetrahedral sites; O, octahedral sites).

inscribed spheres can be considered more as a local gauge of the channels that are formed from an unbroken series of interstitial sites<sup>9</sup> (Figure 2) rather than implying that the form of the pores is necessarily spherical.

In the distribution obtained by Frost from Finney’s model, the pores range from  $K = 0.225$ , corresponding to the void between four tangential spheres. There are no voids present larger than the particle size, that is,  $K < 1$ .

The loose model of Scott is slightly less dense. The pores are more widely distributed and the maximum of the  $p(K)$  distribution occurs for a  $K$  value slightly higher than that of the preceding case.

The  $p(K)$  functions provide a quantitative means of evaluating pore-size distribution. To permit the comparison with experimental  $dV/dr$  pore volume distributions, the distributions  $\psi(K) = K^2 p(K)$  are calculated. These functions are represented in Figure 3. A logarithmic scale for  $K$  is used to facilitate the fitting of the experimental data by simply sliding it along the  $K$  axis until reaching the position considered to give the best fit. The fit allows the particle size of a monodisperse system to be calculated from the maxima of the pore size distributions.

When the Lennard-Jones potential is used, instead of applying the hard-sphere approximation, it should be noted that the  $p(K)$  functions are modified, and two

(8) Zarzycki, J. In *Chemical Processing of Advanced Materials*; Hench, L., West, J. K., Eds.; John Wiley & Sons: New York, 1992; p 84.

(9) Zarzycki, J. *J. Non-Cryst. Solids* **1992**, *147*, 148, 176.

(10) Rodríguez Ortega, J. Ph.D. Thesis, University of Cádiz, Spain, 1996.

(11) Rodríguez-Ortega, J.; Esquivias L. *J. Sol-Gel Sci. Technol.* **1997**, *8*, 117.

(12) Frost, H. *ONR Technical Report No. 6*; Division of Applied Sciences, Harvard University, Cambridge, MA, 1978.

(13) Finney, J. L. *Proc. R. Soc. (London)* **1970**, *A319*, 479.

(14) Finney, J. L.; Wallace, J. *J. Non-Cryst. Solids* **1981**, *43*, 165.

(15) Bernal, J. D.; Mason, J. *Nature* **1960**, *188*, 910.

(16) Scott, G. D. *Nature* **1960**, *188*, 908.

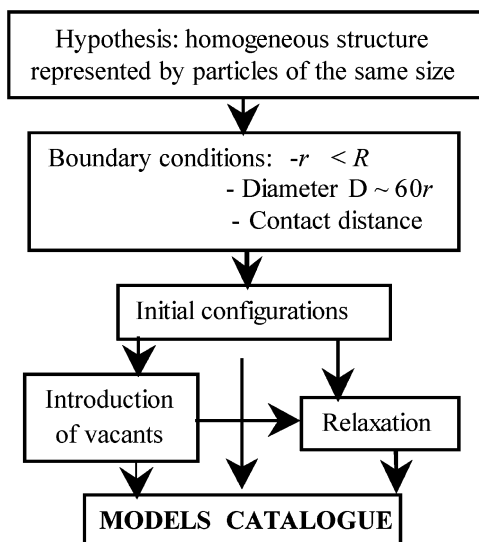


**Figure 4.** Outline of the process followed to generate our catalog of models.

**Table 1. Contact Criteria and Compactness of Models**

type of model	closeness of contact ( $L/d$ )	$C$
H	$0.91 < L/d < 1.00$	0.55
D	$0.95 < L/d < 1.02$	0.52
S	$1.00 < L/d < 1.18$	0.44

maxima emerge corresponding to tetrahedral sites (T) for  $K = 0.225$  and octahedral sites (O) for  $K = 0.414$ .<sup>14</sup>

The model characteristics are expressed as a function of particular macroscopic parameters such as the compactness of the packing,  $C = (\text{spheres volume})/(\text{total volume})$ , and the average coordination number  $N_{CM}$ .  $C$  depends on the definition of the *closeness of the contact* (distance between the centers of two particles/particle diameter,  $L/d$ ) and is almost linearly related by  $N_{CM} \approx 12.7C^{17,18}$  presenting a maximum at  $N_{CM} \approx 8$ . Here we considered it interesting to obtain systematic data on the pore size distribution  $\Psi(K)$ .<sup>10,11</sup> In this respect, a network created from randomly distributed nucleation spots harmonizes better with the intrinsic nature of the gelling kinetics and gel consolidation. Thus, the models are not purely geometric but were submitted to a series of different processes of relaxation and "hollowing out". In this manner, we have created a catalog of pore size distributions to compare them with that of the gels under study, to choose the most appropriate model.

The catalog was generated from three basic spherical models, H, D, and S of diameters  $d \sim 60r$ . Table 1 gives the values for closeness of contact conditions and resulting compactness of each type. In Figure 4 the procedure for generating the model is outlined. In Figure 5 the pore size distributions,  $p(K)$ , of these three basic models are represented.

The S model, as in Scott's loose model, would be formed mainly by octahedra, slightly distorted because the maximum of the distribution is near the octahedral sites. The D model has the maximum population of pores for  $K_{\max} = 0.34$ . This is a consequence of allowing interpenetration or deformation of the spheres. This distribution is intermediate between the Scott and Finney models. The H model allows 10% of radial deformation, giving rise to a model with the maximum of the distribution  $K_{\max} = 0.25$ , a value not very different from that corresponding

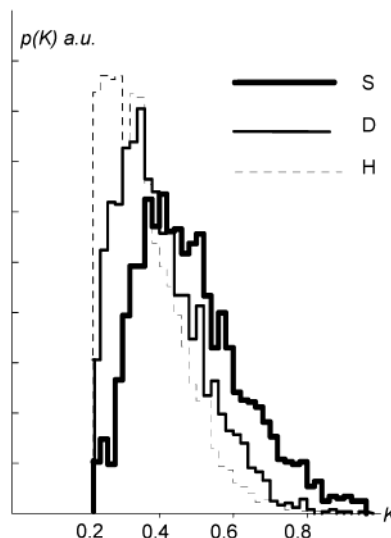


**Figure 5.** Interstice distribution functions for H, D, and S models.  $K = r/R$ , where  $r$  is the radius of the largest inscribed sphere and  $R$  the particle radius.

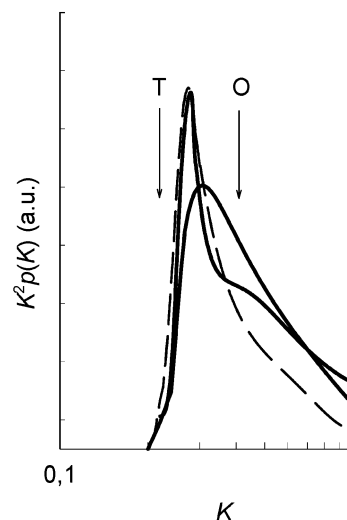


**Figure 6.** Volume derivative distributions  $\Psi(K) = K^2 p(K)$  traced as a function of  $\log K$  corresponding to H20L9 (dashed line), D20L9 (continuous gray line), and S20L9 (continuous black line) models. Positions corresponding to tetrahedral sites (T) for  $K = 0.225$  and octahedral sites (O) for  $K = 0.414$  are indicated.

to the tetrahedral sites. Finney's model has  $K_{\max}$  at 0.3, although it is a little more compact,  $K$  ranging from 0.225 to 0.8.

The models are assisted to converge toward a particular structure by introducing random voids into the structure and relaxing the network, applying the Lennard-Jones potential.<sup>14</sup> A Monte Carlo algorithm finds the distribution of minimum energy. The models are identified as  $XyLz$ , where

$X$  indicates the type of model, H, D, and S,

$y$  is the percentage of added porosity,

$z = 10\sigma$  parameter for Lennard-Jones potential, i.e., L8 means  $\sigma = 0.8$ .

Figure 6 presents the pore volume derivatives of models H20L9, D20L9, and S20L9, that is to say, they have 20% additional porosity and are then relaxed with a Lennard-Jones potential ( $\sigma = 0.9$ ). In ref 6 are included the pore volume derivatives and pore volume distributions of some other models from our catalog and their bidimensional representations.

(17) Ichikawa, T. *Phys. Status Solidi A* **1975**, *29*, 293.

(18) Blétry, J. Z. *Naturforsch., A: Phys. Sci.* **1977**, *32*, 445.

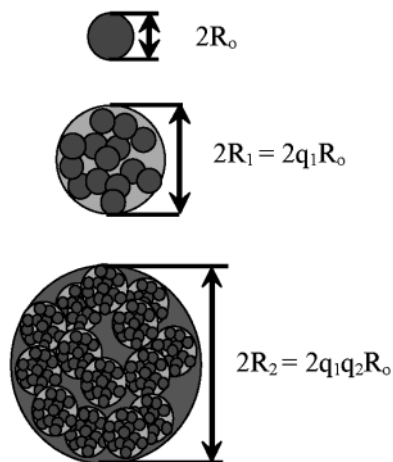


**Figure 7.** Representation of a hierarchic structure.

The experimental distribution can also be decomposed into several portions from which successive sizes and local densities ( $\rho_i$ ) of hierarchic distribution may be deduced.<sup>10</sup> Considering pore volumes  $V_i$  associated with different hierarchic levels and the elementary particle density to be  $\rho_s$ , the local density may be calculated from the general relationship by using

$$V_i = \frac{1}{\rho_i} - \frac{1}{\rho_s}$$

and the successive packing fractions are

$$C_i = \frac{\rho_{i+1}}{\rho_i}$$

In this case, the spheres of the ( $i+1$ )th level,  $R_{i+1}$  radius, are formed by a similar arrangement of smaller spheres of  $R_i$  radius,  $q_{i+1}$  being the radius ratio,  $q_{i+1} = R_{i+1}/R_i$ . These smaller spheres could be also formed by random close-packed spheres of  $R_{i-1} = R_i/q_i$  radius (Figure 7), and so on.

The variable  $K$  at the  $i$ th level,  $K^i$ , is related to the pore size,  $r^i$  and elementary particle size,  $R_0$ , by the relationship

$$K^i = \frac{\rho_i}{R_i} = \frac{\rho_i}{\prod_1^i q_i R_0} \quad (1)$$

We showed, in a preceding paper,<sup>11</sup> that the most appropriate model can be selected from our catalog with the help of an estimate of the  $K$  value at which the model pore volume distribution must have its maximum,  $K_{\max}$ . This is calculated from the position of the maximum of the pore distribution of the  $i$ th level,  $r_{\max}^i$ , and that of the tail of the preceding level,  $r_t^{i-1}$ , by the expression

$$K_{\max}^i \approx 0.8 \frac{r_{\max}^i}{r_t^{i-1}} \quad (2)$$

This value is only a standard, bearing in mind other plausible hypotheses would give a deviation no higher than 10%.

Data on the pore volumes associated with different hierarchical levels, size of aggregates, the local density of the  $i$ th level of aggregation, and packing of the successive levels can be obtained. Table 2 gives the structural

**Table 2.** Structural Parameters of the Models from Our Catalog Employed in This Work<sup>a</sup>

	$K_{\max}$	$C$	$\rho_{\text{RCP}}$ , g/cm <sup>3</sup>	$V_{\text{RCP}}$ , cm <sup>3</sup> /g	$V_m$ , cm <sup>3</sup> of mesopore/g	$N_{\text{CM}}$
HOL7	0.31	0.58	1.28	0.33	0.31	7.66
HOL9	0.28	0.61	1.34	0.29	0.27	8.87
S20L9	0.28	0.38	0.84	0.74	0.32	6.04
S40L9	0.26	0.32	0.68	1.01	0.41	4.89
S60L9	0.26	0.27	0.59	1.23	0.26	4.07

<sup>a</sup>  $K_{\max}$  is the distribution maximum position;  $C$  is the packing fraction;  $\rho_{\text{RCP}}$  is the model specific mass in the case of being formed by silica particles;  $V_{\text{RCP}}$  is the specific volume of the model (RCP);  $V_m$  is the specific mesopore volume, i.e., after subtracting the specific macropore (pores larger than the particle size) volume;  $N_{\text{CM}}$  is the particle average coordination number.

parameters of each particular model from our catalog used in this paper.

We have also applied this technique to Hg porosimetry data of sono-aerogels.<sup>19</sup> We showed that the approach of this method can be extended to another pore range. This only signifies a scale change that is marked by the resolution of the probe. Certainly, when the probe is Hg intrusion, the texture of gel may change. However, this does not imply that we forego taking advantage of the information that can be obtained for increasing our knowledge of the texture, in the absence of isostatic pressure.

## Experimental Section

**Synthesis of the Gels.** This structural study was performed on monolithic colloid–polymer hybrid gels containing various proportions of silica particles, which were prepared following the synthesis method proposed by Toki et al.<sup>20</sup> The colloidal silica selected was Aerosil-OX-50 (Degussa) produced by hydrolyzing  $\text{SiCl}_4$  with an oxy-hydrogen flame. According to manufacturer's specifications, the product is constituted by particles of 40 nm primary average size and presents a specific surface area of 50 m<sup>2</sup>/g. The proportion by weight of  $\text{SiO}_2$  particles to total  $\text{SiO}_2$  was varied between 30%, 54%, 65%, and 82%. (In this paper, we will refer to each particular sample by these percentage numbers.)  $\text{H}_2\text{O}:\text{TEOS}:\text{HCl}$  were mixed in the mole ratio of 10:1:0.001. Next, the sol was subjected to ultrasound action by applying 0.6 W·cm<sup>-3</sup> of ultrasound power for 300 s. Then the appropriate amount of Aerosil was added under vigorous stirring. Finally the pH was raised to 4.5 by adding  $\text{NH}_4\text{OH}$ . For comparison, a sol without addition of colloidal silica was produced following the same preparation process. The gels were dried in an oven at 50 °C. A pinhole aperture limited the drying rate. Gels were maintained in an oven until no change of weight was observed, which occurred in 2 weeks.

**Electron Microscopy.** The composites were examined using scanning electron microscopy (SEM) and transmission electron microscopy (TEM). The observations were performed by using, respectively, the JSM 820 and JEM 2000EX instruments from JEOL installed at the Central Science and Technology facilities in the University of Cádiz.

**Nitrogen Adsorption–Desorption.** The gels were texturally characterized by isothermal nitrogen adsorption–desorption at 77 K in an automatic device. Pore size distributions were calculated by the Horvath–Kawazoe (HK) method<sup>21</sup> up to pore size of 10-nm radius.

**Mercury Intrusion Porosimetry.** To resolve larger pore size, where  $\text{N}_2$  physisorption is not reliable, porosity was also characterized by mercury intrusion on degassed monolithic composites, according to the procedure already described.<sup>7</sup> Hg pressure varied from 0.1 to 390 MPa. After the run, the samples presented both compaction and intruded mercury, except for the

(19) Esquivias, L.; Rodríguez-Ortega, J.; Barrera-Solano, C.; de la Rosa-Fox, N. *J. Non-Cryst. Solids* **1998**, *225*, 239–243.

(20) Toki, M.; Miyashita, S.; Takeuchi, T.; Kanbe, S.; Kochi, A. *J. Non-Cryst. Solids* **1988**, *100*, 479.

(21) Horvath, G.; Kawazoe, K. *J. Chem. Eng. Jpn.* **1983**, *16* (6), 470.

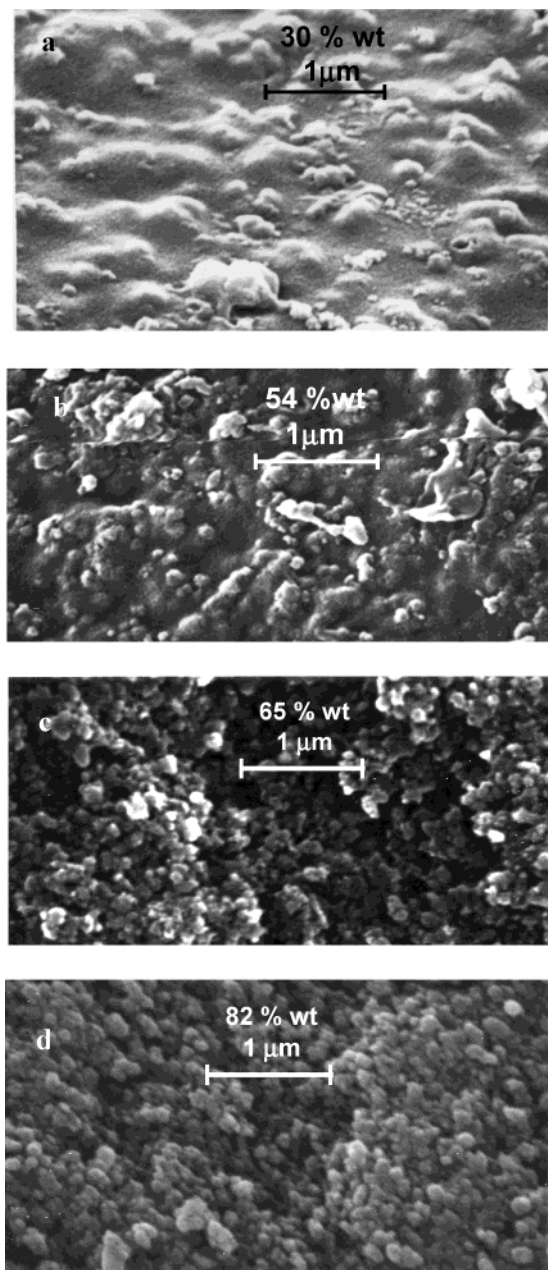


**Figure 8.** SEM micrographs of samples with (a) 30% by weight and (b) 54% by weight of colloid. Both cases can be described as a composite in which the sonogel is the matrix and the colloid is the reinforcing phase. In the samples with (c) 65% by weight and (d) 82% by weight of colloid, the continuous structure of sonogel can no longer be distinguished.

pure sono-xerogel sample and the composite containing 30 wt % of colloid. To determine the volume exclusively due to intrusion, runs were compared with results from specimens encapsulated in a rubber membrane, which prevents the entry of mercury.

They show clearly two superimposed structures: the network of colloid particles and the sonogel matrix, which in these illustrations appears like a mist surrounding the particles.

## Results

**$N_2$  Physisorption Porosimetry Analysis.** The structures in the range of pores smaller than 2 nm radius are entirely due to the sonogel phase. As would be expected, the microporosity is much more important in the pure sonogel and 30% samples than in the other samples. The 30% sample presents a pore distribution quite similar to the pure sono-xerogel, the main difference being that the

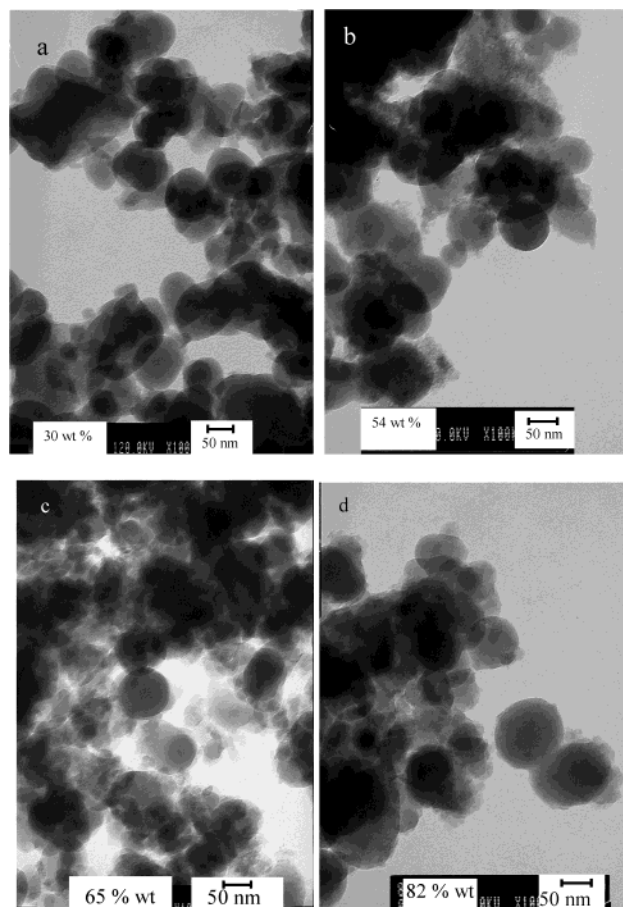


**Figure 9.** TEM observation of gels with (a) 30% and (b) 54% by weight of colloid and samples with (c) 65% and (d) 82% by weight of colloid. In every case the mixing of the coexisting silica phase can be appreciated. The space that surrounds the spherical particles of the colloid is filled by sonogel. Spherical particles are coated by the sonogel phase, as can be seen in the 82% sample.

tail of the distribution is longer in the case of the 30% sample than in the pure sono-xerogel, as can be seen in Figure 10. This experiment does not resolve the pore size in the smallest particle aggregates. The fitting is not possible for radii of less than 1 nm because of the existence of a substantial amount of microporosity, which overlaps the smallest pores of the next higher level of distribution. But this is not a serious impediment, since the particle radius can be estimated from the tail. The radius of the particles, which are actually aggregates of several particles, is 2.8 and 4.2 nm for the pure sono-xerogel and the 30% sample, respectively, with an estimated error of 10%.

Accordingly, the structure of these samples can be described by a uniform distribution of particles of these sizes. The micropores would be formed by elementary particles of < 1-nm radius (estimated from the position of the tail, overlapped by the distribution of the first level), these particles forming the aggregates. Figure 11 is a representation of the structural model of the sono-xerogel phase.

Unlike the other samples with a higher colloid content, in the 30% sample the colloid particles do not contribute to the structure of the gel. They form "islands" in a "sea" of sonogel. This is clearly seen in the corresponding TEM micrograph Figure 9a, where scattered spheres of 80–85-nm diameter can be observed.

The sonogel structure is identifiable in the 54% and 65% samples (Figure 10). The distribution of the 54%

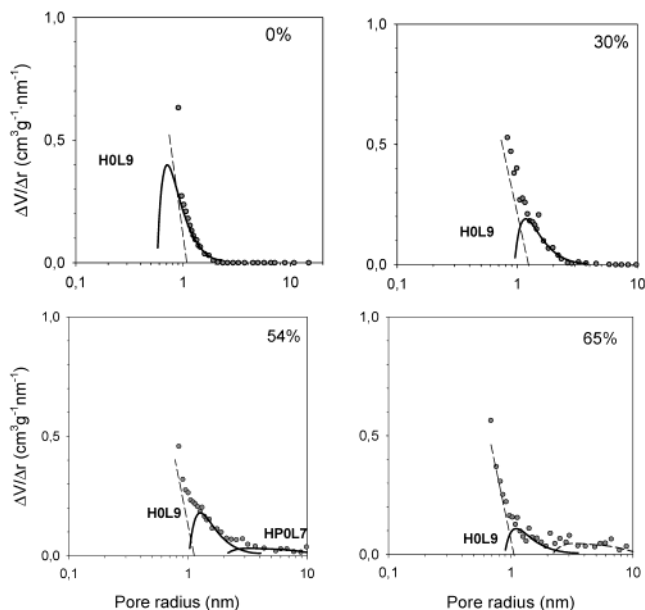


**Figure 10.** Pore size derivatives at the level of the sonogel structure obtained from  $N_2$  physisorption fitted with the models indicated. Dots correspond to the experimental output. Solid lines are the pore distribution of the models applied. The broken line is the proposed tail of the micropore distribution.

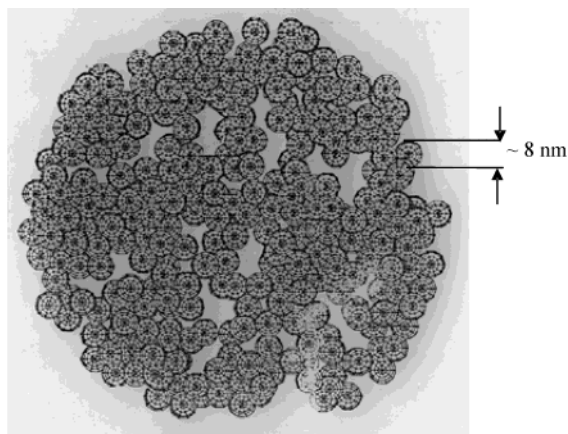


**Figure 11.** Representation of the model of the sono-xerogel phase.

sample can be fitted by two of the more dense and relaxed models of our catalog, HOL9 and HOL7 ( $N_{CM} \sim 8$ ), under the hypothesis of hierarchical distribution. The first level of this distribution corresponds to the elementary particles forming micropores. The dashed line is the proposed tail of the micropore distribution.

The sonogel structure of the 54% and 65% samples consists of particles of  $\sim 4$  nm that are actually aggregates of elementary particles of  $\sim 1$ -nm radius. The porosity described by the model HOL7 corresponds to particles of  $\sim 10$  nm, whether sono-xerogel aggregates or colloid particles. These data contain more noise than those of samples with lower colloid content. The higher concentration of colloid causes the scattering of data because the colloid particles are not monodisperse. The presence of these colloid particles gives rise to porosity at the highest radii that we are examining here. This is especially evident in the 65% sample. The noise/signal ratio along the third level of the 65% sample prevents the differentiation of the most suitable model. To overcome this obstacle, we consider it reasonable to accept the model HOL7. No models have been applied for the 82% sample.

If we know the whole volume enclosed by the aggregates of elementary particles, the density of the  $i$ th level can be calculated as

$$\rho_i = \left( \sum V_i + \frac{1}{\rho_s} \right)^{-1} \quad (3)$$

where  $\rho_s$  is the elementary particle density and  $V_i$  is the pore-specific volume at the  $i$ -th level (analytically calculated). However, a part of that volume could be inaccessible to  $N_2$ . For this reason the relative packing fractions,  $C_i = \rho_{i+1}/\rho_i$  would be overvalued because the density values are calculated by considering that only the measured pore volume exists. As we said above, up to pores of 2-nm radius, only the sonogel could be considered. Thus, our reference value for the measured volume is the amount of sonogel of the corresponding sample,  $V_i^*$ , that permits the calculation of the particular density  $\rho_i^*$  of the sonogel phase at the level  $i$ . Then, the density of the composite is calculated as the weighted average of both phases, considering that, at this level of resolution, the density of the colloid phase is that of the bulk silica, i.e.,  $2.2 \text{ g}\cdot\text{cm}^{-3}$ . The structural parameters calculated from the models applied are included in Table 3.

The pore distribution, calculated from the desorption branch by the Barret-Joyner-Halenda (BJH) method,<sup>22</sup> has been published in our previous article.<sup>7</sup> They present well-defined peaks in the range of pores larger than 5-nm radius. However, our models cannot be properly applied because the polydispersity of the colloid silica phase complicates the problem. This needs a complete study although procedures exist for a possible theoretical approach.<sup>23</sup> Porosity larger than 5 nm corresponds to colloid particles and their agglomerates. A common feature of the distributions of the 54%, 65%, and 82% samples is a peak or shoulder situated at 7–9 nm that mostly corresponds to particles of  $\sim 20$ -nm radius, in agreement with the average primary size of colloid particles provided by the manufacturer. They are coated by sonogel and aggregates of very small sonogel particles. The sonogel is also accommodated in the interstices of the colloid particles and, consequently, the peak of the main feature narrows. In Figure 9c, numerous particles of colloid can be identified. Their surface is not smooth because they are coated by sonogel. The TEM micrograph Figure 9c of the 65% sample gives a good view of this.

In Figure 9d (TEM micrograph of the 82% sample), agglomerates of colloid particles as well as individual colloid particles can be seen. In the corresponding SEM micrograph (Figure 8d) large agglomerates (100–200 nm radius) can also be seen.

**Hg Intrusion Porosimetry Analysis.** An appropriate resolution in the largest pore size is given by Hg porosimetry. We characterized the pore structure from Hg intrusion data according to the pore distribution calculated from the classic Washburn interpretation. As shown in Figure 12, the maximum of the experimental distribution shifts toward higher values (from 15 to 28 nm) as the colloid content increases, whereas the feature of porous volume associated with lower values of pore radius was maintained fairly constant. Porosity also increases. The pore radius distributions present a clearly defined maximum close to a prominent shoulder sloping down toward lower pore sizes, where the relative maxima are around 3.8 nm.<sup>7</sup> The models S60L9, S20L9, and S40L9 of our

(22) Barret, E. P.; Joyner, L.; Halenda, P. P. *J. Am. Chem. Soc.* **1951**, *73*, 373.

(23) Dodds, J. A. *J. Colloid Interface Sci.* **1980**, *77*, 317.

**Table 3. Structural Parameters of the Sonogel Model Calculated from the Models Applied<sup>a</sup>**

sample	model	level 1							$q_1$	level 2		
		$r_1$	$\rho_1$	$\rho_1^*$	$C_1^*$	$V_1$	$V_1^*$	model		$r_2$	$\rho_2$	$V_2$
54	HOL9	4.3	1.78	1.28	0.58	0.150	0.326	~4	HOL7	10.5	1.40	0.153
65	HOL9	3.9	1.90	1.36	0.65	0.099	0.282	~4	HOL7	10.5	1.63	0.086

<sup>a</sup>  $r_i$ , nm;  $\rho_i$ , g·cm<sup>-3</sup>;  $V_i$ , cm<sup>3</sup>/g of composite;  $V_i^*$ , cm<sup>3</sup>/g of sonogel.

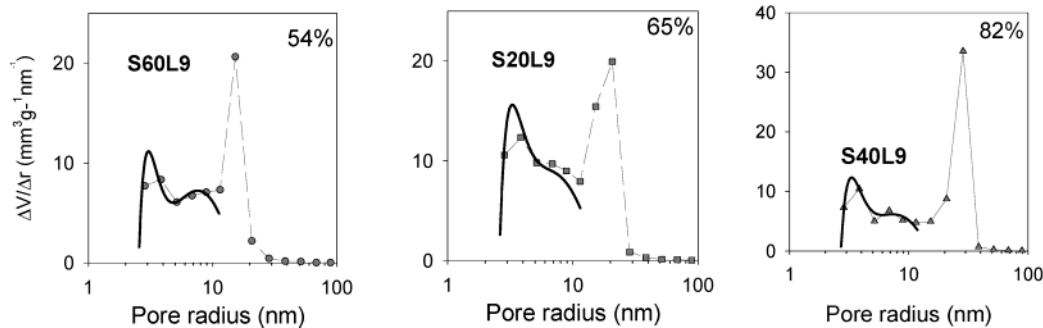


**Figure 12.** Derived pore sizes obtained from Hg intrusion porosimetry. Dots correspond to the experimental data; the dashed lines between them are only a guide for visual purposes. Solid lines are the pore distribution of the model applied.

**Table 4. Calculated Structural Parameters for the Distributions Calculated from Hg Porosimetry Data<sup>a</sup>**

sample	level 0	level 1				level 2			bulk	
	$V_\mu$ , cm <sup>3</sup> /g ( )	model	$r_1'$	$\rho_1'$	$V_1'$	$V_1'/V_m$	$\rho_2'$	$C_2'$	$V_2'$	$\rho_a$
54%	0.129 (16.6 %)	S60L9	12.4	1.94	0.067	0.25	1.53	0.79	0.133	1.26
65%	0.112 (12.4 %)	S20L9	11.1	1.93	0.065	0.16	1.29	0.67	0.256	1.11
82%	0.079 (7.7 %)	S40L9	12.2	1.98	0.051	0.12	1.08	0.56	0.407	0.97

<sup>a</sup>  $r_i'$ , nm;  $\rho_i'$ , g·cm<sup>-3</sup>;  $V_i'$ , cm<sup>3</sup>/g. The accent on the figure is only to indicate that these measurements correspond to Hg porosimetry.  $V_\mu$  (cm<sup>3</sup>/g) ( ); in parentheses, the percentage of the total volume of the sample.

catalog can satisfactorily replace these features for the 54%, 65%, and 82% samples, respectively. The calculated structural parameters are shown in Table 4. This has to be understood as a volume fraction of the sample given by the ratio between the measured volume and  $V_m$  of the applied model, shown in Table 2; it is produced by the geometry depicted. That is to say, this is a network of particles of  $r_1'$  radius, with a coordination number  $N_{CM}$  between 4 and 6.

These models are relatively uncoordinated and relaxed. According to their  $K_{max}$  included in Table 2, the radius of the aggregates ranges between 11 and 12 nm. This value could correspond both to agglomerates of sonogel particles and to colloid particles. In view of the decreasing value of the fraction  $V_1'/V_m$  (the accent has been added to the figure only to indicate that these measurements correspond to Hg porosimetry) for decreasing sono-xerogel content, we consider that this structure is formed predominantly by this phase of the composite. The sonogel particles that form these aggregates would be closely packed as a consequence of the isostatic pressure. Pores below 2 nm cannot be identified because this is the threshold of resolution of the experiment. Pores of this size may be found within those aggregates. We have calculated the densities  $\rho_1'$ . The differential of  $\rho_2'$  with respect to the bulk density is due to the sample compaction caused by both the isostatic pressure and the porosity being below 2-nm radius, with pores apparently situated between the elementary particles of the sonogel. This differential becomes larger for increasing sono-xerogel content, because the internal porosity characteristic of the sonogel aggregates also increases. The reduction of volume caused by isostatic pressure at  $P_1$  ( $P_1$  is the intrusion pressure), in accordance with results presented in our previous paper,<sup>7</sup> is 0.011, 0.014, and 0.026 cm<sup>3</sup>/g for the 54%, 65%, and 82% samples, respectively. From these measurements, the micropore volume ( $V_\mu$  in Table 4) is

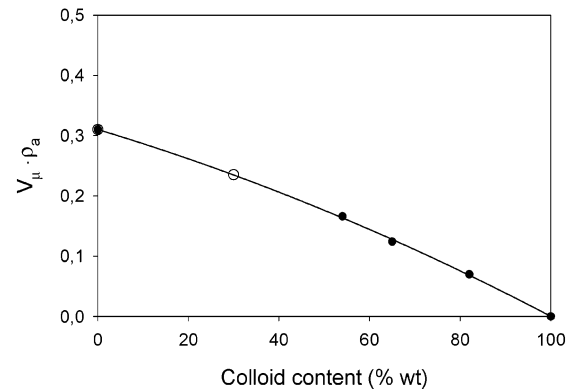


**Figure 13.** Quadratic fitting between micropore volume ( $\rho_a V_\mu$ ) relative to the sample volume vs colloid content. Open circle is the interpolated value for the 30% sample

calculated. Figure 13 represents the fraction of micropore volume ( $\rho_a V_\mu$ ) vs colloid content in each of the samples under study. A good quadratic fitting is obtained, as can be appreciated. Interpolation of these data permits a micropore volume of 0.18 cm<sup>3</sup>/g (23% of the total volume of the sample) to be inferred for the 30% sample. This calculation is made assuming that a pure colloid sample would never have pores of less than 2-nm radius and, on the other hand, the pore radii of the pure sono-xerogel sample are all less than 2 nm (Figure 10). Undoubtedly, the decreasing amount of fine porosity for a decreasing concentration of the polymeric phase is the reason of the increase of compliance.<sup>7</sup>

The largest pores observed with this technique are ~40 nm in radius, whereas in the measurements with N<sub>2</sub> physisorption, pores of radius larger than 100 nm were observed. From the narrowness of the peaks, it can be accepted that they are due to the pores formed by aggregates of sonogel situated in the pores between colloid

particles. The pore volume ( $V_2$ ) at this level increases when the colloid content increases, as would be expected. High colloid content also contributes to the formation of large aggregates. The larger the aggregates, the larger the pores between them. Thus, for increasing colloid content, the space available to accommodate sonogel increases, but the available amount of sonogel, obviously, decreases as well. Consequently, this results in an increase of the pore size in the range of pores between the colloid particles. The density evaluated at level 2, at which pore distribution is due to the combined structure of sonogel and colloid particles, is nearer to the apparent bulk density for increasing colloid content, since the porosity inaccessible to Hg (basically caused by the sonogel phase) decreases with colloid content.

### Conclusions

1. It has been possible to extract structural information on these composites from  $N_2$  physisorption and Hg intrusion data, by means of models constructed using Monte Carlo calculations, on the basis of random close packing (RCP) premises.

2. The characteristic uniform structure of silica colloid gel undergoes profound modification when it is mixed with silica sonogel.

3. The structure of gels with 30% and 54% by weight of colloid can be described as a composite in which the sonogel is the matrix and the colloid is the reinforcing phase. The structure is continuous at the scale of the observation.

4. Samples with 65% and 82% by weight of colloid are discontinuous and colloid aggregates of 110–120-nm radius are observed. Aggregates larger than 200-nm radius are also observed in the 82% sample.

5. The micropore volume existing within sonogel aggregates has been estimated. It decreases from 31% of the total volume of the pure sono-xerogel sample to 7.7% of the 82% sample.

6. The collapse of the structure produced by isostatic pressure gives rise to agglomerates of sonogel particles of ~11–12 nm. There is a reduction of the colloid pore size by compaction of this structure.

**Acknowledgment.** We are grateful for financial support from the Spanish Government: Ministerio de Ciencia y Tecnología (Projects MAT2001-3805 and MAT2002-0859) and Junta de Andalucía (TEP 0115). We are also grateful to Degussa Iberia, S.A., for supplying Aerosil OX-50.

LA035248R